analytical chemistry

Article

pubs.acs.org/ac

Concurrent Detection of Cellular and Molecular Cancer Markers Using an Immunomagnetic Flow System

Wanfeng Huang,[†,‡] Chun-Li Chang,[†,‡] Bin-Da Chan,[†,‡] Shadia I. Jalal,[⊥,#] Daniela E. Matei,[⊥,#] Philip S. Low,[§] and Cagri A. Savran*[,†,‡,∥]

[†]Birck Nanotechnology Center, [‡]School of Mechanical Engineering, [§]Department of Chemistry, and [∥]Weldon School of Biomedical Engineering, Purdue University, West Lafayette, Indiana 47907, United States

[⊥]Department of Medicine, Indiana University School of Medicine, Indianapolis, Indiana 46202, United States

[#]Indiana University Simon Cancer Center, Indianapolis, Indiana 46202, United States

Supporting Information

ABSTRACT: We report a detection system for simultaneous measurement of cellular and molecular markers of cancer. Magnetic beads conjugated with antibodies against a specific antigen are used to capture both free molecules and whole cells overexpressing the antigen. The target-bound beads then flow through a microfluidic chamber where they are drawn to a glass surface by an external magnetic field. The cells and molecules captured on the surface are quantitatively analyzed using fluorescent microscopy. The system was characterized by detecting free folate receptor (FR) and an FR+ cancer cell line (KB) in culture media. The system detected as low as 10 pM of FR and captured 87% of the spiked KB cells at a volumetric throughput of 3 mL/min. We further demonstrated the detection of 100 KB cells and 200 pM FR spiked into healthy human blood to simulate detection of rare cells and protein biomarkers present in a cancer patient's blood sample. The FR concentration was measured to be 244 pM (including the intrinsic FR present in the blood), and the total number of KB cells in the sample was estimated to be 98. The potential of this approach in clinical diagnostics was also demonstrated by detecting both FR+ cells and free FR in an ascites sample obtained from an ovarian cancer patient. Because of the system's capability to detect multiple targets at the same time, its high throughput, and its overall simplicity, we expect it to be highly useful in a wide range of research settings.

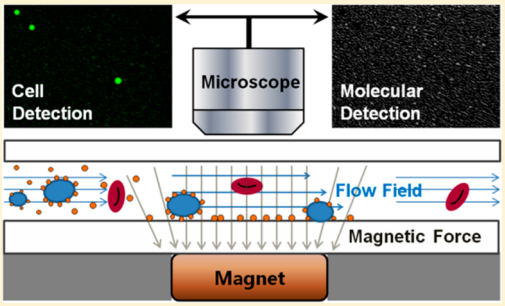

Isolating cells from biological fluids has always been important in a number of fields such as cell biology, physiology, medicine, and pathology. Cell sorting techniques are routinely applied to separate cells of interest from heterogeneous suspensions.[1] For example, isolation and detection of circulating tumor cells (CTCs) has been shown to predict treatment efficacy and has the potential to become a marker for early detection of cancer.[2−5]

Detecting molecular biomarkers is also important in diagnosis, prognosis, and selection of therapy for particular diseases. Protein biomarkers in serum can reveal significant information about the onset and progression of many diseases ranging from heart failure to cancers.[6,7] For instance, a number of studies showed that folate receptor (FR, also known as folate binding protein) is a biomarker for several epithelial malignancies.[8−10] It has also been shown that ovarian cancer patients have elevated serum levels of FR α, which is overexpressed on the surfaces of malignant cells and eventually shed into the blood.[11]

Thanks to the advance of micro- and nanofabrication techniques there are many methods currently available for rare cell detection including inertial focusing, fluorescence-activated cell sorting (FACS), microchip-based immunomagnetic methods, and microaperture chip system for high-throughput cell detection.[1,5,12−14] There are also numerous approaches available for biomolecule detection, such as fluorescence immunoassays, enzyme-linked immunosorbent assays (ELISAs), surface plasmon resonance (SPR), quartz crystal microbalance (QCM), microcantilever detection, and diffraction-based biosensors.[15−19]

Although it is possible to adapt some molecular detection platforms to detect whole cells, and vice versa, most platforms are optimized for detection of either molecules or cells but not both. Often, multiple devices are used to perform each test separately at different times and/or with different samples. We herein present an approach to simultaneously capture and quantify both cells and biomolecules from the same sample fluid.

Our system uses magnetic particles functionalized with antibodies against target biomolecules as well as surface antigens on target cells and captures the bead-bound targets on a chip surface using high flow rates. The method is versatile enough that various groups of beads can be combined to

Received: February 9, 2015
Accepted: July 11, 2015
Published: July 12, 2015

DOI: 10.1021/acs.analchem.5b02215
Anal. Chem. 2015, 87, 10205−10212

recognize various molecular targets and cell surface antigens. The method becomes especially simple for applications wherein the free biomolecular target is also overexpressed on the target cell surface, e.g., free prostate-specific membrane antigen (PSMA) and PSMA+ tumor cells, and free epidermal growth factor (EGFR) and EGFR+ tumor cells. In this study we chose free folate receptor (FR) and FR+ tumor cells as our model dual targets to demonstrate the concept of concurrent detection. KB cells are known for overexpressing high level of FR and hence were used in this study as a model to mimic FR+ tumor cells present in cancer patients' bodily fluids.

MATERIALS AND METHODS

The detection strategy is illustrated in Figure 1. Superparamagnetic particles are first conjugated with polyclonal antibodies against FR (anti-FR). These anti-FR beads are then introduced into a sample fluid containing FR and KB cells for incubation (Figure 1a). The incubated sample mixture then flows through a fluidic chamber made of a poly(dimethylsiloxane) (PDMS) channel and two glass slides (Figure 1b) at a flow rate of 3 mL/min. During the flow, target cells and molecules are attracted to the surface of the bottom glass slide by a magnetic field generated by a magnet placed beneath the chamber, while other entities in the sample fluid are washed away under a high volumetric flow (3 mL/min). Finally, captured targets are quantitated by using fluorescence microscopy.

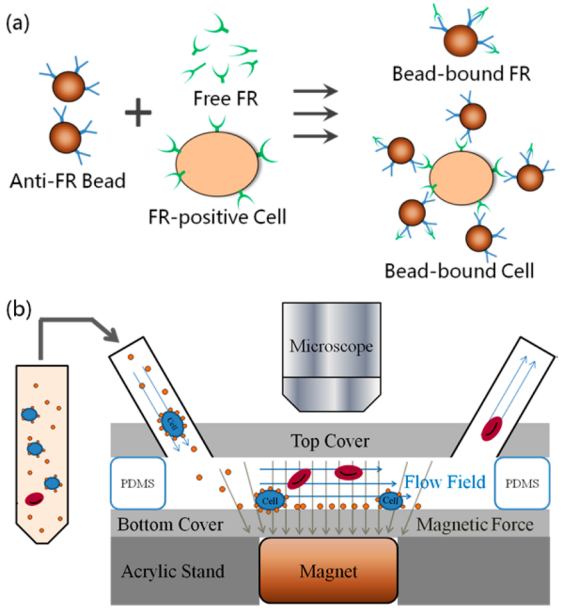

Figure 1. Schematic showing the operation principles: (a) FR molecules and FR+ KB cells bound to anti-FR beads; (b) microfluidic chamber designed for immunomagnetic detection of KB cells and free FR: KB cells and FR are simultaneously captured by the magnetic field as the sample fluid flows through the chamber.

In this study we first modeled the forces within the system and numerically simulated the resulting particle trajectories to understand favorable operating conditions. The system was then characterized in terms of its response to free protein concentration, as well as its yield in detecting cells spiked in complex mixtures. To demonstrate the system's potential in clinical applications, we detected free FR and KB cells spiked into healthy human blood, as well as endogenous FR and FR+ cells present in the ascites obtained from an ovarian cancer patient.

System Setup. The picture of the experimental setup and the components of the fluidic device are shown in Supporting Information Figure S-1. The fluidic channel (length, 25.4 mm, × width, 3.8 mm, × height, 1.5 mm) was constructed by patterning a cured PDMS layer using a computer-controlled CO_2 laser cutting system (Universal Laser System, Inc. Professional Series) and covering the PDMS pattern with two glass slides on the top and the bottom. The assembled chamber was sealed by a pair of acrylic cover and stand using screws and nuts. A neodymium permanent magnet (K&J Magnetics, grade N52 with a flux density of 6451 G at the magnet surface) was inserted into the groove of the acrylic stand to provide a magnetic field from the bottom of the chamber (illustrated in Figure 1b and Supporting Information Figure S-1b). A peristaltic pump (New Era Pump Systems, NE-9000) was utilized to draw sample fluid into the chamber and then to a waste container.

Preparation of FR Antibody-Coupled Magnetic Beads. To prepare the anti-FR beads, streptavidin-coated 1 μm magnetic beads (20 μL, 10 mg/mL, Sigma-Aldrich) were incubated with biotinylated polyclonal antibodies against FR (10 μL, 0.2 mg/mL, R&D Systems) in a phosphate-buffered saline (PBS) solution at room temperature for 1 h. After incubation, the beads were washed three times with PBS using a magnetic stand to remove unbound antibodies and resuspended in 100 μL PBS.

Preparation of KB Cells and FR. FR+ KB cells, obtained from American Type Culture Collection, were cultured in folic acid depleted RPMI 1640 medium (Gibco, U.S.A.) with 10% fetal bovine serum (FBS). Before the spiking process, KB cells were harvested using trypsin−EDTA (Invitrogen) and resuspended in culture medium. Cell concentration was measured by taking five samples (each with a volume of 3 μL) and manually counting the cell number to obtain an average. The suspensions were subsequently spiked into medium or blood to achieve the desired concentrations.

Recombinant human folate receptor (FR) was purchased from R&D Systems and stored at −20 °C with a concentration of 100 μg/mL in PBS. FR was diluted and added into medium or blood to desired concentrations for characterization and detection experiments.

Blood Samples for KB and FR Spiking Experiments. Blood was collected from healthy volunteers under an approved IRB protocol. Deidentified blood samples were drawn and collected in BD vacutainer tubes with additives of sodium poly(anethol) sulfonate (SPS). Blood samples were kept at 4 °C immediately after collection until the spiking process. Blood samples were used within 12 h after being collected (usually within 4 h) to ensure the viability of blood cells.

Ascites Sample for Dual-Target Detection. Ascites from a recurrent ovarian cancer patient with stage IIIC high-grade serous primary peritoneal carcinomatosis was collected at the Indiana University Hospital under an approved IRB protocol, and kept at −20 °C until experimentation. Prior to processing the ascites fluid was thawed and filtered (pore size, 100 μm) to remove large impurities in the fluid.

Fluorescent Staining for Free FR and FR+ Cell Quantification. Earlier studies have shown that fluorescein isothiocyanate-conjugated folate, i.e., folate−FITC, is effective in imaging FR+ malignant tumors with very low background in FR− malignant or benign lesions.[20] In this study, 10 μM of

DOI: 10.1021/acs.analchem.5b02215
Anal. Chem. 2015, 87, 10205−10212

folate−FITC was used to stain both free FR molecules and FR + cells captured by the anti-FR beads. Free FR molecules were sandwiched between the folate−FITC and the anti-FR on the beads. While detecting cells, folate−FITC not only made it easier to identify whole cells on the glass surface but also served as an independent check for FR positivity (in addition to the antibody-mediated bead binding which can be observed in bright field). For characterization experiments performed in media, folate−FITC was incubated with captured targets under static conditions at room temperature for 1 h. For analysis of bodily fluids, 34 nM of CD45 monoclonal antibodies conjugated with phycoerythrin (anti-CD45-PE, Abcam, U.S.A.) and 0.18 μM of 4′,6-diamidino-2-phenylindole (DAPI, Sigma-Aldrich, U.S.A.) were also introduced in addition to folate−FITC to recognize white blood cells and to identify nucleated cells.

For experiments that involved blood, red blood cell (RBC) lysis buffer (G-Biosciences, U.S.A.) was introduced into the chamber after the cell capturing process and incubated for 5 min to remove residual RBCs. Cells captured on the glass surface were then fixed using 4% paraformaldehyde (PFA, Santa Cruz Biotechnology, U.S.A.) in PBS. Folate−FITC, anti-CD45-PE, and DAPI were subsequently introduced into the fluid chamber and incubated under static conditions at room temperature for 1 h. After incubation, the fluidic chamber was washed with PBS at a flow rate of 4 mL/min for 30 s and was subjected to fluorescence microscopy for enumeration of the cancer cells as well as quantification of FR concentration.

RESULTS AND DISCUSSION

Modeling and Simulation. We generated a computer-based numerical simulation using the COMSOL Multiphysics 4.3a modeling software. We first modeled the magnetic and fluidic fields inside the fluidic chamber and defined the primary forces acting on an entity inside the chamber. Then a particle trajectory module (PTM) was used to obtain the trajectories of 300 beads and 30 cell−beads complexes.

To simplify the simulation we assumed that the internal magnetization between the particles, the influence of the particles on the fluidic field, and the coupling between the fluidic and the magnetic fields were negligible. Also, the magnitude of the magnetic force acting on a cell−beads complex was assumed to be directly proportional to the total number of the beads attached to the cell. According to the fluidic channel dimensions and the flow properties, the Reynolds number was calculated to be Re = 18.87. Therefore, the flow was considered to be laminar (Re < 2100). We also assumed that particles (free beads and bead−cell complexes) were randomly distributed over the cross section of the inlet tube when they were about to be released into the chamber.

Our model included two types of particles: free beads and cell−beads complexes. To simulate the motion of a particle in the chamber, we applied the Newton's second law to each particle:

$$m\frac{\partial \vec{V}}{\partial t} = \vec{F}_m + \vec{F}_d + \vec{F}_g + \vec{F}_b \quad (1)$$

where $\vec{V}$ is the velocity of the particle and m is the mass of the particle, which could be either a single free bead or a bead−cell complex. The average mass of a dry KB cell, which is approximately 30% of the original mass, was measured to be 760 pg using a cantilever-based resonator.[21] Hence, the mass of a single "wet" cell was taken as 2533 pg, which is in reasonable agreement with a previous study.[22] The mass of a single magnetic bead with 1 μm diameter is around 1 pg. Thus, the mass of a cell bound with N beads is 2533 + N pg.

The buoyant force $\vec{F}_b$ can be expressed by

$$\vec{F}_b = -\rho \vec{g} V \quad (2)$$

where ρ is the density of the fluid (1000 kg m^{-3}), $\vec{g}$ is the gravitational acceleration, and V is the volume of the particle (2.4×10^{-15} m^3 for a cell−beads complex and 5.2×10^{-19} m^3 for a single bead). The buoyant forces applied on a free bead and a KB cell are about 0.005 and 24 pN, respectively (the latter number also holds for cell−bead complexes where N < 100).

$\vec{F}_g$ is the weight of the particle:

$$\vec{F}_g = m\vec{g} \quad (3)$$

Hence, the total gravity force on a KB cell or a KB cell−bead complex is around 25 pN (for N < 100).

The magnetic force induced on a particle ($\vec{F}_m$) is estimated by[23,24]

$$\vec{F}_m = N\frac{V\chi}{2\mu_0}\nabla(\vec{B}\cdot\vec{B}) \quad (4)$$

where V is the volume of the particle, χ = 2.7 is the effective volumetric magnetic susceptibility, μ_0 is the vacuum permeability, and $\vec{B}$ is the magnetic flux density, which is shown in Figure 2a. N is the number of beads attached to a cell and is equal to 1 for the case of a free bead. The resulting magnetic force applied on a bead at the detection surface in the chamber is shown in Figure 2b. The blue solid line represents lateral magnetic force, whereas the green dash line represents the vertical magnetic force.

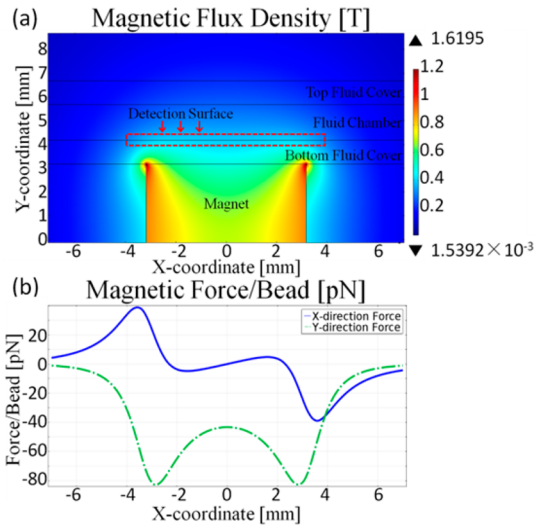

Figure 2. (a) Color map of the simulated magnetic flux density with a magnitude range from 0.2 to 1.2 T and (b) the corresponding magnetic force induced on a single bead on the detection surface. The blue solid line shows the force in the X (lateral) direction while the green dashed line indicates the force in the Y (vertical) direction.

Our experimental observations indicate that the number of beads bound to a single cell is highly variable (from ∼10 to a

DOI: 10.1021/acs.analchem.5b02215
Anal. Chem. 2015, 87, 10205−10212

few hundred, see Supporting Information Figure S-2). For our subsequent simulations we considered the lower end of this range where N = 10 beads/cell to account for a conservative scenario. The magnetic force applied on a bead depends on its position in the chamber, and the maximum magnetic force applied on a single KB cell bound to 10 beads can be as high as 800 pN.

The fluidic drag force on the particle is given by[24]

$$\vec{F}_d = 6\pi\eta r_p(\vec{U} - \vec{V}_p) \quad (5)$$

where η is the fluid dynamic viscosity (10^{-3} kg m^{-1} s^{-1}), r_p is the radius of particle (0.5 μm for a single bead and 8.3 μm for a complex), $\vec{U}$ is the velocity of fluid, and $\vec{V}_p$ is the velocity of particle. The drag force applied on a KB cell with 10 beads ranges from 0 to 500 pN and is influenced by the difference between the particle velocity and the surrounding fluid velocity at different positions and time.

On the basis of eqs 1−5, a finite element simulation was used to investigate the effect of flow rates on the trajectories of both free beads and cell−beads complexes inside the fluidic chamber. In the simulation the particles were assumed to terminally halt once they contact the chamber surface, and the locations were recorded for analysis of optimal flow rate. Figure 3a shows the simulation of the final distribution of 300 superparamagnetic beads on the detection surface at a flow rate of 3 mL/min. Also shown are micrographs taken from different locations on the chip surface after an experiment performed under the same conditions (only the number of beads used in the simulation was deliberately kept small to reduce computation time). Figure 3b shows the simulation results where 30 KB cell−bead complexes (blue dots) along with 300 free beads (red dots) were introduced into the chamber under various flow rates. The capture rate of bead-bound KB cells was calculated accordingly by dividing the number of cells arriving at glass surface to the total number of cells introduced and was plotted against the flow rate in Figure 3c. This figure shows that when flow rate is as high as 4 mL/min, the system starts to lose cells. On the other hand, when the flow rate is too low (<2 mL/min), even though theoretically the cell recovery rate should be high, we observed that the beads tend to accumulate in small areas, resulting in practical difficulties in imaging and discriminating cells. The optimized balance between throughput and cell recovery rate can be achieved at a flow rate of 3 mL/min.

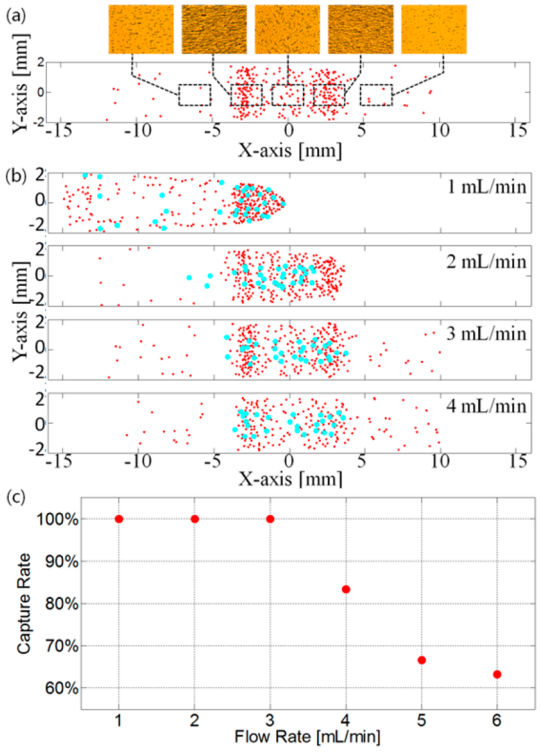

Figure 3. (a) Simulated distribution of beads under a 3 mL/min flow rate, as well as experimental micrographs from five locations on the chip. (b) Simulated distributions of beads (red dots) and bead-bound-KB cells (blue dots) under flow rates of 1, 2, 3, and 4 mL/min. (c) Simulated capture rate of bead-bound KB cells with various flow rates (each cell was assumed to have 10 beads attached).

System Characterization for Molecular Detection. We first characterized the system for detection of molecular markers only by detecting known concentrations of FR added into 1 mL of cell culture medium. 20 μL (40 μg) of anti-FR beads were incubated with the samples at room temperature for 1 h to capture the free FR. The mixture was then flowed through the detection chamber at a flow rate of 3 mL/min, and the magnetic beads were pulled down and held on the detection surface by the magnetic field. Following that, the chamber was rinsed with PBS to wash away unbound FRs and impurities. The accumulated beads were subsequently incubated with folate−FITC for 1 h at room temperature to stain the FR captured on the beads for fluorescent analysis. Figure 4 shows the fluorescent and corresponding bright field micrographs of the beads captured on the glass surface with three different FR concentrations, 100, 1, and 0 nM.

To study the relationship between the input (FR concentration) and output (fluorescence) signals, we calculated the total fluorescence intensity in an observation window and subtracted the background intensity observed in a bead-free area in the same window. This fluorescence intensity was then

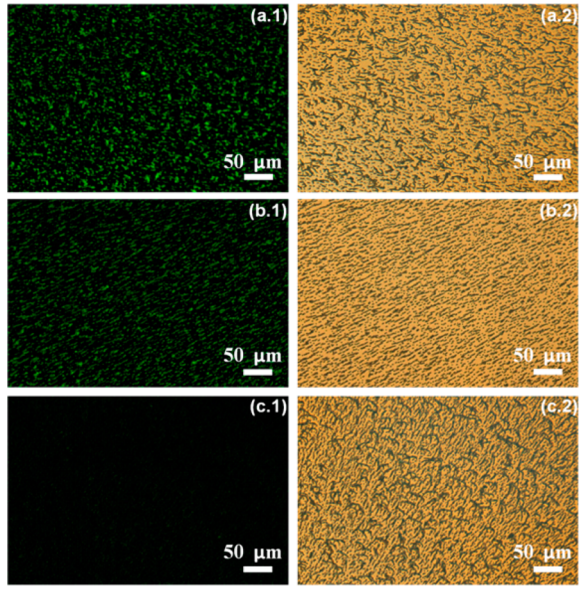

Figure 4. Fluorescent and bright field images collected from samples with different FR concentrations. Image pairs a, b, and c were captured from samples with FR concentrations of 100, 1, and 0 nM, respectively. All the fluorescent images were equally enhanced for display.

DOI: 10.1021/acs.analchem.5b02215
Anal. Chem. 2015, 87, 10205−10212

normalized by the intensity of the reverse bright field image, which represents the number of the beads on the detection surface. The resulting signal, called the "B-ratio", is a measure of the fluorescence signal per bead (see Supporting Information Figure S-3 for more details). We measured the B-ratio obtained from eight various FR concentrations starting from 0 to 200 nM and plotted the results in Figure 5. For each measurement

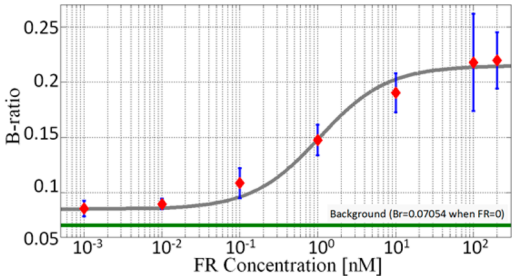

Figure 5. Variation of fluorescence with FR concentrations from 1 pM to 200 nM. Error bars represent standard deviations from three measurements. Green horizontal line represents experimental background (B-ratio when FR = 0). Solid curve is the Langmuir isotherm fit.

three images were acquired at different locations of the glass surface. Performing a least-squares Langmuir isotherm fit to the experimental data revealed:

$$B_r = \frac{0.1299}{1 + 1.055/C_f} + 0.08504 \quad (6)$$

where B_r is the B-ratio, C_f is the FR concentration, and 0.08504 is the theoretical bias which could result from the nonspecific binding between folate−FITC and anti-FR beads and/or the intrinsic fluorescent background of the magnetic beads (which agrees with our experimentally observed B-ratio bias of 0.071). The dissociation constant K_d between anti-FR and FR was found to be around 1.055 nM, which is in agreement with previous reports.[25,26] Figure 5 also shows that the dynamic range of this system for detecting FR covers the free FR levels mostly observed in blood samples of ovarian cancer patients: 70 pM to 2 nM.[19,27,28] We were able to detect concentrations as low as 10 pM [with a 3 SD (standard deviation) difference from the background]. Although we were also able to measure lower signals at 1 pM, such signals did not differ significantly from that of 10 pM.

Characterization of the System by Detecting FR+ Cells in the Presence of Free FR. We next characterized the system for simultaneous detection of both cellular and molecular targets. Around 100 KB cells and FR molecules with concentrations between 1 pM and 100 nM were spiked in cell culture medium with a volume of 1 mL. The mixture was then incubated with 20 μL (40 μg) of anti-FR beads for 1 h at room temperature before flowing through the fluidic device for detection. Following that, the fluidic chamber was subjected to folate−FITC staining and fluorescent microscopy to quantify the two targets detected on the glass surface. To eliminate the influence of the fluorescence signal coming from the cells on free FR quantification, the images of cells were deliberately removed from both fluorescent and bright field images before calculating the B-ratio (Figure 6).

The detection yields of the KB cells and the measured FR concentrations are plotted against the concentration of free FR spiked in medium in Figure 7. We observed a monotonic

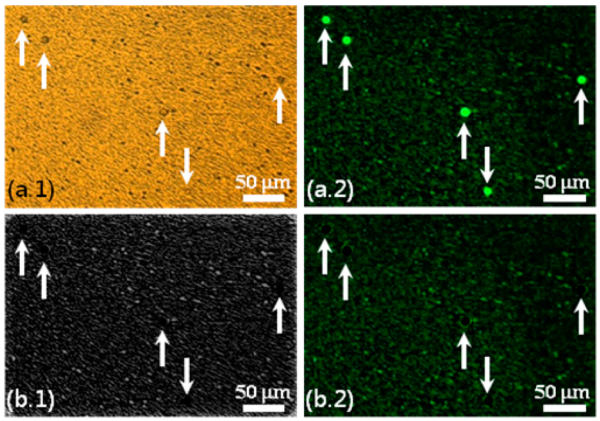

Figure 6. Bright-field (a.1, b.1) and fluorescent (a.2, b.2) images obtained from the same detection surface. In images b.1 and b.2 cells were deliberately removed for B-ratio calculation. Image b.1 is a reverse bright field image in grayscale. White arrows point to the locations of the captured cells.

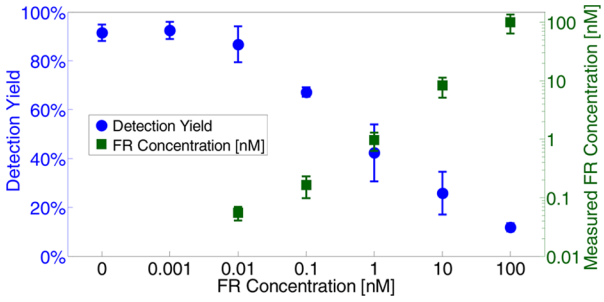

Figure 7. Detection yield of KB cells and the measured free FR concentration plotted against spiked FR concentration. Blue circles represent the cell detection yield while green squares represent the measured FR concentration. Error bars indicate standard deviations for three measurements.

relationship between spiked and measured free FR concentrations. The free FR concentration was estimated by comparing the measured B-ratio to the Langmuir isotherm fit described by eq 6. Therefore, the systematic accuracy of the estimated concentration is limited by how well the fit represents the calibration data with respect to how much the data varies in a specific concentration region. For example, for concentrations between 10 and 100 pM, as well as above 10 nM, the slope of the fit is relatively small, and hence, errors in B-ratio could result in larger errors in the estimated concentration. The difference between the Langmuir fit and the actual data can also lead to overestimation of the concentrations at the lower end of the dynamic range.

In Figure 7 the cell detection yield remains above 90% when the FR concentrations were below 10 pM. However, the detection yield starts to decrease with increasing FR concentration above 10 pM. We attribute this to a competition effect between the KB cells and the free FR molecules, whose quantity and mobility is higher than that of the cells. A high level of free FR therefore masks the beads' binding sites and lowers the number of FR+ cells captured by the beads (on the other hand, the presence of cells does not significantly hamper the capturing of molecules). Therefore, the plot in Figure 7 serves as a calibration curve to estimate the original number of cells present in a sample fluid based on the number of cells

DOI: 10.1021/acs.analchem.5b02215
Anal. Chem. 2015, 87, 10205−10212

captured on the chip surface and the measured FR concentration.

We verified that a fluorescent signal coming from a FR+ cell is primarily due to the FR on the cell itself by imaging KB cells that is not exposed to any beads (see Supporting Information Figure S-4). We also performed a negative control experiment wherein we used the same procedures in KB cell detection to attempt capturing 4T1 cell line (Life Technologies) that is known to be FR-negative.[29] Only 1.4% of 4T1 cells were found on the detection surface (see details in Supporting Information Figure S-5).

Concurrent Detection of Molecules and Cells Spiked into Blood Samples. To study the potential of the system for clinical applications, FR and KB cells were spiked into blood samples collected from a healthy donor. An amount of 500 μL of unprocessed whole blood was first diluted with PBS to 2 mL. Around 100 KB cells were spiked into the diluted blood sample along with 200 pM of free FR. The mixture was incubated with 20 μL (40 μg) of anti-FR beads at 4 °C for 90 min. Each sample was then flowed through the fluidic chamber (under the influence of the magnetic field) at a flow rate of 3 mL/min, which was followed by washing with 3 mL of PBS. After the detection process, red blood cell (RBC) lysis buffer (G-Biosciences, U.S.A.) was introduced into the fluidic chamber and incubated for 5 min to remove residual RBCs. The sample was then subjected to fluorescence staining and microscopy while still in the chamber. We identified KB cells based on a combination of factors including the size (10−30 μm) and shape (close to circular) of the observed cells and their fluorescent emissions, wherein a folate−FITC(+), anti-CD45-PE(−), and DAPI(+) cell was scored as a positive result. Figure 8 shows the fluorescent images of three KB cells and a leukocyte, as well as FR-beads captured on the glass slide in the chamber.

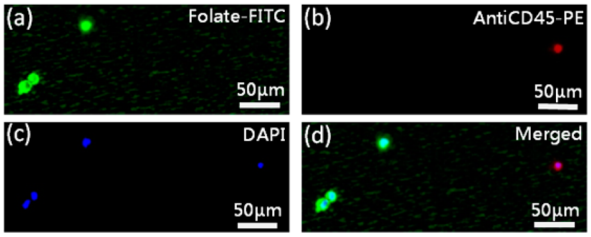

Figure 8. Fluorescent micrographs showing KB cells as well as free FR detected from blood: (a) KB cells stained by folate−FITC; (b) leukocytes stained by anti-CD45-PE; (c) cell nuclei stained by DAPI; (d) a merged image of panels a−c. Images were enhanced for clarity of display.

The FR level of the blood was measured to be 244 pM, which is slightly higher than the FR concentration we spiked in (200 pM). This finding could be attributed to the endogenous FR present in healthy blood (the FR level present in unspiked blood was measured to be 27 pM). The number of KB cells captured on the chip was counted to be 62. On the basis of the measured FR level and the KB detection yield in Figure 7, the estimated total number of KB cells present in blood was calculated to be 98, which is very close to the number of cells spiked in the sample (100).

Concurrent Detection of Free FR and FR+ Tumor Cells in Ascites Fluid. The system was finally challenged to detect FR and FR+ cells present in bodily fluids obtained from a cancer patient. For this purpose ascites was obtained from a patient with stage IIIC ovarian cancer (high-grade serous primary peritoneal carcinomatosis). An amount of 1 mL of filtered malignant ascites was first diluted to 4 mL with PBS buffer. Following the protocol described previously but without adding any free FR or KB cells, intrinsic FR+ cells and free FR were captured and fluorescently stained for identification and quantification. Once again, only those cells showing folate−FITC+, DAPI+, and anti-CD45− were scored (those cells that appeared triple-positive, i.e., folate−FITC+, DAPI+, and CD45+, were excluded from scoring). We captured 43 FR+ cells and measured 940 pM of FR from the diluted sample (i.e., 3.8 nM FR for the original sample, Supporting Information Figure S-6). Using the free FR concentration along with the calibration data in Figure 7, the original number of FR+ cells present in the 1 mL of ascites can be estimated to be around 101. These data demonstrate the capability of the system to be applied to clinical samples.

To verify the results obtained using our system, FR concentration and number of FR+ cells present in the same ascites sample were also determined using ELISA and flow cytometry, respectively. An ELISA kit for FR measurement was purchased from R&D Systems (Human FLOR1 Quantikine ELISA kit, DFLR10). Following the protocols provided by the vendor, various concentrations of standard folate receptor included in the kit were first used to generate a reference curve (see details in Supporting Information Figure S-7). An amount of 200 μL of ascites sample was diluted by 100-fold, and then 50 μL of diluted sample was measured based on the reference curve. The resulting FR concentration of the diluted ascites was measured to be 44.7 pM, which yields an FR concentration of 4.5 nM in the original ascites. This value is in reasonable agreement with the FR concentration measured by our system (3.8 nM).

To detect FR+ cells in the ascites sample using flow cytometry, a total volume of 1 mL of ascites was first diluted to 2 mL with PBS buffer and separated into two tubes. Following that, 10 μM of folate−FITC was introduced and incubated for 30 min to stain FR+ cells. All mixtures were then centrifuged, and the supernatants were aspirated. The cell pellets were suspended in 250 μL of PBS buffer before introducing into a flow cytometer (BD Biosciences, ACCURI C6). The total number of folate−FITC+ cells was 167, in comparison with what we estimated using our system (101 cells). The difference could be attributed to the following reasons: (1) In our system we observed and excluded some triple-positive cells (folate−FITC+, DAPI+, and CD45+), which would normally be counted by a flow cytometer that simply scores all FITC+ cells. (2) The calibration curve in Figure 7 was obtained for a specific type of cell that has a high expression of FR and hence can result in underestimating the number of other cells if they have a weaker expression of FR. (3) Since the concentration of target cells sought is relatively small (only some 100 within some milliliters), it is possible that two separate volumes, even if they come from the same original sample, may not contain exactly the same number of cells. Given these possibilities, the difference in the number of cells estimated in the two independent experiments is reasonable.

In the future our system can effectively be extended to other biomarkers as well as diseases. For example, interesting comparative studies can be performed where free PSMA as well as PSMA+ circulating tumor cells (CTCs) are detected simultaneously and all in one sample. Similarly, one can detect

DOI: 10.1021/acs.analchem.5b02215
Anal. Chem. 2015, 87, 10205−10212

the CA125 molecular marker as well as FR+ CTCs in ovarian cancer patient samples. These studies may provide insight into the relative importance of each type of target with respect to the other, correlations between the levels of two types of targets, and how this correlation is related to the progression of the disease.

CONCLUSION

We have presented a simple immunomagnetic system capable of simultaneous detection of free molecules and whole cells. We demonstrated the concept by applying the system to detection of free FR molecules as well as FR+ cells. The optimal flow rate was found to be 3 mL/min based on a computational model, and the system was characterized using this flow rate by detecting both molecular and cellular targets spiked in cell culture medium. The dynamic range of FR detection was found to be between 10 pM and 100 nM, whereas the detection yield of KB cells was found to be dependent on the FR concentration due to a competition effect between both targets. Therefore, a calibration curve was obtained to use the number of cells captured on the chip surface along with the measured FR concentration to estimate the number of cells in the original sample fluid. We also showed the concurrent measurement of FR and KB cells spiked in healthy blood, which demonstrated the potential of this system in clinical applications. Finally we applied this system to the analysis of a bodily fluid obtained from a cancer patient, where we detected free FR as well as FR + cells endogenously present in the ascites fluid of an ovarian cancer patient. The detection results obtained using our system, which could detect both molecules and cells concurrently, were comparable with those obtained using ELISA to detect molecules only and those obtained using flow cytometry to detect cells only. Lastly, the concept on which this system is built on is generic and versatile, and hence, the same principles could be applied to detection of a wide range of cells and molecular biomarkers present in various bodily fluids.

ASSOCIATED CONTENT

Supporting Information

System setup (Figure S-1), number of beads per KB cell (Figure S-2), algorithm of B-ratio calculation (Figure S-3), fluorescent images of KB cells (Figure S-4), detection yields of 4T1 and KB cells (Figure S-5), measurement of ascites samples (Figures S-6 and S-7), and particle initial distribution and simulated capture rate (Figures S-8 and S-9). The Supporting Information is available free of charge on the ACS Publications website at DOI: 10.1021/acs.analchem.5b02215.

AUTHOR INFORMATION

Corresponding Author

*E-mail: savran@purdue.edu.

Notes

The authors declare no competing financial interest.

ACKNOWLEDGMENTS

This work was supported by a TRASK Innovation Fund from the Purdue Research Foundation and the National Science Foundation Grant 1343069.

REFERENCES

(1) Hu, X. Y.; Bessette, P. H.; Qian, J. R.; Meinhart, C. D.; Daugherty, P. S.; Soh, H. T. *Proc. Natl. Acad. Sci. U. S. A.* **2005**, *102*, 15757−15761.
(2) Cristofanilli, M.; Hayes, D. F.; Budd, G. T.; Ellis, M. J.; Stopeck, A.; Reuben, J. M.; Doyle, G. V.; Matera, J.; Allard, W. J.; Miller, M. C.; Fritsche, H. A.; Hortobagyi, G. N.; Terstappen, L. W. *J. Clin. Oncol.* **2005**, *23*, 1420−1430.
(3) Danila, D. C.; Heller, G.; Gignac, G. A.; Gonzalez-Espinoza, R.; Anand, A.; Tanaka, E.; Lilja, H.; Schwartz, L.; Larson, S.; Fleisher, M.; Scher, H. I. *Clin. Cancer Res.* **2007**, *13*, 7053−7058.
(4) Krebs, M. G.; Metcalf, R. L.; Carter, L.; Brady, G.; Blackhall, F. H.; Dive, C. *Nat. Rev. Clin. Oncol.* **2014**, *11*, 129−144.
(5) Ozkumur, E.; Shah, A. M.; Ciciliano, J. C.; Emmink, B. L.; Miyamoto, D. T.; Brachtel, E.; Yu, M.; Chen, P. I.; Morgan, B.; Trautwein, J.; Kimura, A.; Sengupta, S.; Stott, S. L.; Karabacak, N. M.; Barber, T. A.; Walsh, J. R.; Smith, K.; Spuhler, P. S.; Sullivan, J. P.; Lee, R. J.; Ting, D. T.; Luo, X.; Shaw, A. T.; Bardia, A.; Sequist, L. V.; Louis, D. N.; Maheswaran, S.; Kapur, R.; Haber, D. A.; Toner, M. *Sci. Transl. Med.* **2013**, *5*, 179ra47.
(6) Weinberg, E. O.; Shimpo, M.; Hurwitz, S.; Tominaga, S.; Rouleau, J. L.; Lee, R. T. *Circulation* **2003**, *107*, 721−726.
(7) Ludwig, J. A.; Weinstein, J. N. *Nat. Rev. Cancer* **2005**, *5*, 845−856.
(8) Yu, Y.; Chen, Z. L.; Dong, J. S.; Wei, P.; Hu, R. J.; Zhou, C. C.; Sun, N.; Luo, M.; Yang, W. J.; Yao, R.; Gao, Y. B.; Li, J. G.; Yang, G. H.; He, W.; He, J. *Translational Oncology* **2013**, *6*, 697−702.
(9) Kalli, K. R.; Oberg, A. L.; Keeney, G. L.; Christianson, T. J. H.; Low, P. S.; Knutson, K. L.; Hartmann, L. C. *Gynecol. Oncol.* **2008**, *108*, 619−626.
(10) O'Shannessy, D. J.; Somers, E. B.; Maltzman, J.; Smale, R.; Fu, Y. S. *SpringerPlus* **2012**, *1*, 22.
(11) Basal, E.; Eghbali-Fatourechi, G. Z.; Kalli, K. R.; Hartmann, L. C.; Goodman, K. M.; Goode, E. L.; Kamen, B. A.; Low, P. S.; Knutson, K. L. *PLoS One* **2009**, *4*, e6292.
(12) Cho, S. H.; Godin, J. M.; Chen, C. H.; Qiao, W.; Lee, H.; Lo, Y. H. *Biomicrofluidics* **2010**, *4*, 43001.
(13) Hoshino, K.; Huang, Y. Y.; Lane, N.; Huebschman, M.; Uhr, J. W.; Frenkel, E. P.; Zhang, X. J. *Lab Chip* **2011**, *11*, 3449−3457.
(14) Chang, C.; Jalal, S.; Huang, W.; Mahmood, A.; Matei, D.; Savran, C. *IEEE Sens. J.* **2014**, *14*, 3008−3013.
(15) Soukka, T.; Paukkunen, J.; Harma, H.; Lonnberg, S.; Lindroos, H.; Lovgren, T. *Clin. Chem.* **2001**, *47*, 1269−1278.
(16) Kucera, E.; Kainz, C.; Tempfer, C.; Zeillinger, R.; Koelbl, H.; Sliutz, G. *Anticancer Res.* **1997**, *17*, 4735−4737.
(17) McKie, A.; Samuel, D.; Cohen, B.; Saunders, N. A. *J. Immunol. Methods* **2002**, *270*, 135−141.
(18) Wu, G. H.; Datar, R. H.; Hansen, K. M.; Thundat, T.; Cote, R. J.; Majumdar, A. *Nat. Biotechnol.* **2001**, *19*, 856−860.
(19) Acharya, G.; Chang, C. L.; Doorneweerd, D. D.; Vlashi, E.; Henne, W. A.; Hartmann, L. C.; Low, P. S.; Savran, C. A. *J. Am. Chem. Soc.* **2007**, *129*, 15824−15829.
(20) van Dam, G. M.; Themelis, G.; Crane, L. M. A.; Harlaar, N. J.; Pleijhuis, R. G.; Kelder, W.; Sarantopoulos, A.; de Jong, J. S.; Arts, H. J. G.; van der Zee, A. G. J.; Bart, J.; Low, P. S.; Ntziachristos, V. *Nat. Med.* **2011**, *17*, 1315−U1202.
(21) Chan, B. D.; Icoz, K.; Huang, W.; Chang, C. L.; Savran, C. A. *Lab Chip* **2014**, *14*, 4188−4196.
(22) Park, K.; Jang, J.; Irimia, D.; Sturgis, J.; Lee, J.; Robinson, J. P.; Toner, M.; Bashir, R. *Lab Chip* **2008**, *8*, 1034−1041.
(23) Shevkoplyas, S. S.; Siegel, A. C.; Westervelt, R. M.; Prentiss, M. G.; Whitesides, G. M. *Lab Chip* **2007**, *7*, 1294−1302.
(24) Furlani, E. P.; Ng, K. C. *Phys. Rev. E* **2008**, *77*, 061914.
(25) O'Shannessy, D. J.; Somers, E. B.; Albone, E.; Cheng, X.; Park, Y. C.; Tomkowicz, B. E.; Hamuro, Y.; Kohl, T. O.; Forsyth, T. M.; Smale, R.; Fu, Y. S.; Nicolaides, N. C. *Oncotarget* **2011**, *2*, 1227−1243.
(26) Sequeira, J. M.; Ramaekers, V. T.; Quadros, E. V. *Clin. Chem. Lab. Med.* **2013**, *51*, 545−554.
(27) Leung, F.; Dimitromanolakis, A.; Kobayashi, H.; Diamandis, E. P.; Kulasingam, V. *Clin. Biochem.* **2013**, *46*, 1462−1468.

DOI: 10.1021/acs.analchem.5b02215
Anal. Chem. 2015, 87, 10205−10212

(28) Parker, N.; Turk, M. J.; Westrick, E.; Lewis, J. D.; Low, P. S.; Leamon, C. P. *Anal. Biochem.* **2005**, *338*, 284−293.
(29) Reddy, J. A.; Westrick, E.; Santhapuram, H. K.; Howard, S. J.; Miller, M. L.; Vetzel, M.; Vlahov, I.; Chari, R. V.; Goldmacher, V. S.; Leamon, C. P. *Cancer Res.* **2007**, *67*, 6376−6382.

DOI: 10.1021/acs.analchem.5b02215
Anal. Chem. 2015, 87, 10205−10212